UNIVERSITY OF CALIFORNIA
IRVINE

CENTER FOR PERVASIVE COMMUNICATIONS AND COMPUTING

GRADUATE FELLOWSHIP PROJECTS PROGRESS REPORTS FALL 2007

PROJECTS

ALPHABETIZED ACCORDING TO STUDENT LASTNAME

STUDENT NAME	PROJECT TITLE	ADVISOR
LUAY AZZAM	DECODING COMPLEXITY OF QUASI-ORTHOGONAL SPACE-TIME CODES	ENDER AYANOGLU
ALIREZA S. BEHBAHANI	OPTIMIZING MIMO RELAY NETWORKS	AHMED ELTAWIL
VIVEK CADAMBE	OPTIMAL INTERFERENCE ALIGNMENT FOR WIRELESS NETWORKS	SYED A. JAFAR
FATEMEH FAZEL	PRACTICAL CODE DESIGN FOR RECONFIGURABLE MIMO SYSTEMS	HAMID JAFARKHANI
MINAS GJOKA	NOVEL USES AND MISUSES OF PEER-TO-PEER SYSTEMS	ATHINA MARKOPOULOU
AMIN JAHANIAN	AN ULTRAHIGH-SPEED ANALOG-TO-DIGITAL CONVERTER (ADC) IN 130NM CMOS	PAYAM HEYDARI
MAHYAR KARGAR	ADAPTIVE EQUALIZATION OF MULTIMODE FIBER CHANNELS IN 0.13µM CMOS	MICHAEL GREEN
AMIN KHAJEH DJAHROMI	CHALLENGES AND OPPORTUNITIES IN DESIGNING ULTRA EFFICIENT COMMUNICATION SYSTEMS IN HIGHLY SCALED TECHNOLOGIES	AHMED ELTAWIL
SEUNG EUN LEE	POWER-AWARE INTERCONNECTION NETWORK FOR WIRELESS MOBILE SYSTEMS	NADER BAGHERZADEH
MOHAMMAD A. MAKHZAN	FAULT TOLERANT VOLTAGE SCALABLE CACHES	FADI KURDAHI
NEGAR NEJATI	OPTIMAL TRANSMISSION OF PACKETIZED VIDEO OVER TANDEM CHANNEL	HAMID JAFARKHANI
HULYA SEFEROGLU	NETWORK CODING FOR PRACTICAL APPLICATIONS OVER WIRELESS MESH NETWORKS	ATHINA MARKOPOULOU
VOLKAN SEVINDIK	USE OF BEAMFORMING IN ORTHOGONAL FREQUENCY DIVISION MULTIPLEXING	ENDER AYANOGLU
SRINIVASAN SURENDRAN	CAN INTERFERENCE ALIGNMENT *DOUBLE* THE CAPACITY OF AN INTERFERENCE NETWORK *WITH CHANNEL UNCERTAINTY ANDLIMITED POWER*?	SYED A. JAFAR

Progress Report on ML Decoding of OSTBC Research: Fall 2007

Luay Azzam, Advisor: Ender Ayanoglu
Center for Pervasive Communications and Computing
Department of Electrical Engineering and Computer Science
The Henry Samueli School of Engineering
University of California, Irvine
Irvine, California 92697-2625
Email: lazzam@uci.edu

***Abstract*— We propose a low complexity Maximum Likelihood (ML) decoding algorithm for orthogonal space-time block codes (OSTBCs) based on the real-valued lattice representation and QR decomposition. In General, ML decoding of OSTBCs is simple since an independent detection of one complex symbol is being decoded at a time. However, we were able to further simplify that decoding complexity and showed that for square L-QAM constellations, this complexity is reduced from $\mathcal{O}(L)$ for conventional ML to $\mathcal{O}(\sqrt{L})$ in this work.**

I. Introduction

In Fall 2007, we focused on the decoding complexity of Orthogonal space-time block codes (OSTBCs). These codes are attractive since they achieve the maximum diversity, the maximum coding gain, and the highest performance [1]. They are used in multiple-input multiple-output (MIMO) systems to introduce large coding gains [2]. Their design allows simple Maximum Likelihood (ML) decoding. The decoding complexity is very critical for practical employment of MIMO systems. In OSTBCs proposed by Alamouti [3] and Tarokh *et al.* [4], each transmitted symbol is decoded separately, resulting in linear decoding complexity. However, this simple decoding complexity can be further reduced. During this quarter, we analyzed the conventional ML decoding, and introduced an alternative new decoding algorithm for square QAM constellations based on the QR decomposition of the real-valued lattice representation and showed that the optimal ML performance can be obtained with a substantial reduction in the decoding complexity. We also compared our decoding complexity with that of conventional ML detection.

To support our analysis, we provide a complexity comparison between conventional ML decoding and our proposed algorithm.

II. Computational Complexity

In this section, the overall complexity is measured in terms of the number of operations required to decode the transmitted signals for each block period T. A complex multiplication is equivalent to 4 real multiplications R_M and 2 real additions R_A, while a complex addition is equivalent to 2 real additions. We split the complexity formula into two parts in order to represent R_M and R_A independently. We denote the complexity of our proposed algorithm by $\mathcal{C}_{PR}$, and show it as a two dimensional vector where the first dimension is the number of real multiplications and the second, the number of real additions, then

$$\mathcal{C}_{PR} = 2K\sqrt{L}(4R_M, 2R_A). \tag{1}$$

Performing QR decomposition and the calculation of some intermediate steps requires additional number of computations Therefore, (1) is rewritten as

$$\begin{aligned}\mathcal{C}_{PR} = &(MT(20K+2) + 12 + 8K\sqrt{L})R_M, \\ &(MT(4K+2) + 2K(2\sqrt{L}-1) - 1)R_A.\end{aligned} \tag{2}$$

Conventional ML detection [5], on the other hand, performs simple detection for each complex symbol independently. The complexity $\mathcal{C}_{ML}$ can be derived using the presentation in [5]

$$\begin{aligned}\mathcal{C}_{ML} = L((&4MN(T+K) + 12K)R_M, \\ &(4MN(T+K) + 6K)R_A).\end{aligned} \tag{3}$$

Obviously, the complexity of ML is $\mathcal{O}(L)$ whereas the complexity of the proposed algorithm is $\mathcal{O}(\sqrt{L})$. We give a comparison between $\mathcal{C}_{PR}$ and $\mathcal{C}_{ML}$ in terms of R_M and R_A considering 2 transmit antennas for different constellation sizes. In Table I, we show this comparison for a 2×1 system employing the Alamouti OSTBC.

TABLE I
# of real multiplications and real additions vs L for 2×1 system using Alamouti code

	L	4	16	64	256
R_M	ML	224	896	3584	14336
	PR	128	160	224	352
R_A	ML	176	704	2816	11264
	PR	31	47	79	143

Clearly, the complexity gain obtained by the proposed algorithm is substantial. Finally, it is important to emphasize the fact that the complexity reduction becomes greater as L is larger.

REFERENCES

[1] H. Jafarkhani, "Space-Time Coding: Theory and Practice," 2005.
[2] N. Al-Dhahir, C. Fragouli, A. Stamoulis, W. Younis, and A. Calderbank, "Space-Time Processing for Broadband Wireless Access," *IEEE Communications Magazine*, vol. 40, pp. 136–142, Sep. 2002.
[3] S. Alamouti, "A Simple Transmit Diversity Technique for Wireless Communications," *IEEE J. on Selected Areas in Communications*, vol. 16, pp. 1451–1458, Oct. 1998.
[4] V. Tarokh, H. Jafarkhani, and A. Calderbank, "Space-Time Block Codes from Orthogonal Designs," *IEEE Trans. Inf. Theory*, vol. 45, no. 5, pp. 1456–1467, Jul. 1999.
[5] ——, "Space-Time Block Coding for Wireless Communications: Performance Results," *IEEE J. on Selected Areas in Communications*, vol. 17, pp. 451–460, Mar. 1999.

Progress Report on "MIMO Relay Networks" Fall 2007

Alireza S. Behbahani, Advisor: Prof. Ahmed Eltawil
Electrical Engineering Department
University of California, Irvine, USA
Email: sshahanb@uci.edu

Relay networks have received considerable attention recently, especially when limited size and power resources impose constraints on the number of antennas within a wireless sensor network. In this context, signal processing techniques play a fundamental role, and optimality within a given relay architecture can be achieved under several design criteria. It has been shown that the use of MIMO wireless networks significantly improves spectral efficiency and link reliability through spatial multiplexing and space-time coding respectively. Figure 1 shows a MIMO relay network where the source and destination each are equipped with M antenna and also there K relays where each is equipped with n antennas. and intra-relay cooperation is further allowed. Previously we designed optimal relay matrixes under several optimal criteria such as minimum mean square error (MMSE), Signal to noise ratio (SNR), and zero forcing (ZF) with and without power constraint.

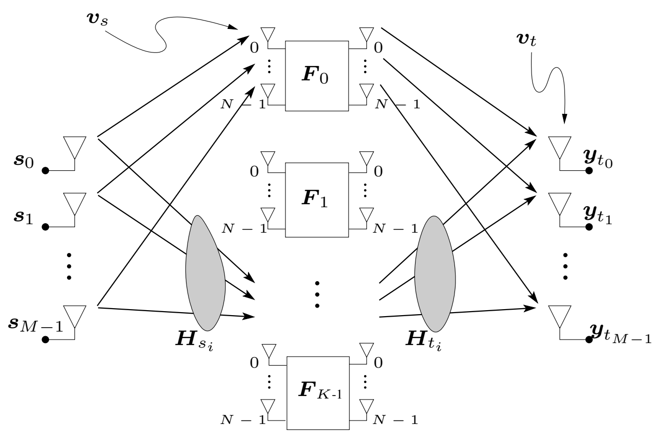

Fig. 1. *MIMO Relay Architecture with intra-relay cooperation.*

Then during Fall 2007, we extended our work to the case of multiple sources and multiple destinations. First we considered a MIMO relay network such that there are L sources and L destinations each equipped with M antennas and such that each source will communicate with a specific destination. We derived optimal relay matrixes under MMSE constraint and compared it with ZF relaying scheme introduced in the literature. Figure 2 shows BER performance of the proposed system compared to ZF for the same total relays output power. As it shows this proposed scheme outperforms ZF scheme. We also considered a MIMO relay network with one source and L destinations each with M antennas and also again K relays each equipped with N antennas. We derived optimal relay matrixes under MMSE constraint without power constraint such that the optimal solution determines the total relay output power. Figure 3 shows BER performance for different number of relays.

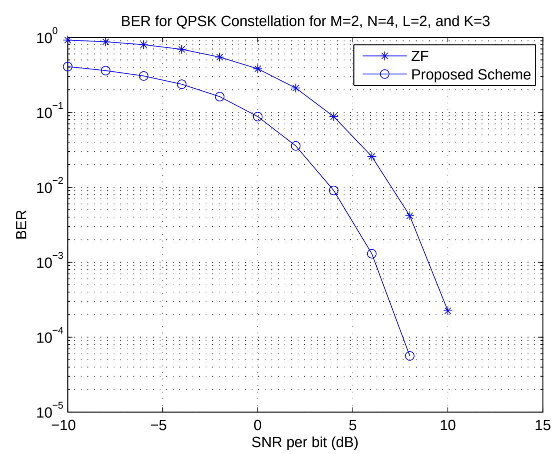

Fig. 2. BER performance of proposed scheme, multiple sources and destinations, and ZF s.t. power constraint (PC) of 4.8 dB for 3 relays.

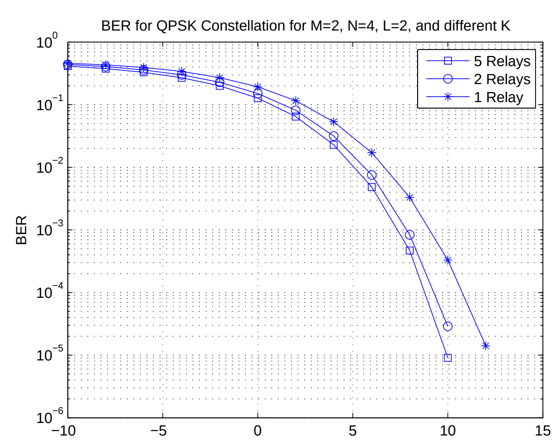

Fig. 3. BER performance of proposed scheme, one source and multiple destinations, without power constraint (PC) for different number of relays.

Progress in Fall 2007 : The capacity of the X channel within $o(\log(\text{SNR}))$

Viveck R. Cadambe, Syed A. Jafar
Center For Pervasive Communications and Computing Electrical Engineering and Computer Science
University of California Irvine,
Irvine, California, 92697, USA
Email: vcadambe@uci.edu, syed@uci.edu

***Abstract*— An X channel is a generalization of the interference network to a scenario where every transmitter has a message to every receiver in the network. In fall 2007, we study the capacity of the X channel with M transmitters and N receivers with MN messages - one message from every transmitter to every receiver in the network. In our previous work, using an achievable scheme based on *interference alignment*, we approximated the capacity of the K user interference channel as $(K/2)\log(\mathbf{SNR}) + o(\log(\mathbf{SNR}))$, or equivalently, we showed that the interference channel has $K/2$ degrees of freedom. In fall 2007, we generalized this result to obtain the degrees of freedom characterization of the X channel with an achievable scheme solving the optimal interference alignment problem (over random channels).**

I. Introduction

In previous work, we showed that the K user interference channel has $K/2$ degrees of freedom meaning that the capacity of the interference network may be written as

$$C(\text{SNR}) = (K/2)\log(\text{SNR}) + o(\log(\text{SNR}))$$

where SNR represents the signal-to-noise ratio. The achievable scheme was based on the idea of interference alignment (see [2] and references therein) - the idea that interfering signals from several transmitters align causing overlapping shadows at the receiver, so that they 'appear' like the signal from a single transmitter. The result demonstrated the power of the technique of interference alignment in combating interference - the primary bottleneck of throughput of wireless networks. In fall 2007, we generalized the results of [1] to X networks.

II. The X network

X networks (earlier studied in [2], [3]) are a generalization of interference networks. Unlike the interference network where a transmitter has a message only to its corresponding receiver, in an X network, there is a message from every transmitter in the network to every receiver. Figure 1 shows the $M \times N$ X network i.e. an X network with M transmitters, N receivers and a message from each transmitter to each receiver resulting in a total of MN messages.

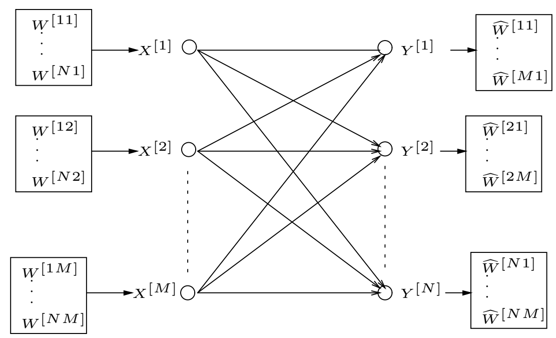

Fig. 1. The $M \times N$ X network

The constraints of the interference alignment problem are much stricter in the X channel since there many more messages, as compared to the interference channel. In fall 2007, we formulated the degrees of freedom characterization of the X channel with an achievable scheme solving the optimal interference alignment problem (over random channels). X networks are interesting because they encompass most one-way single hop communication scenarios. For example, the multiple access, broadcast, and interference channels can be derived from the X network by setting appropriate messages to null. Therefore, the (approximate) capacity characterization of the X network reveal several interesting insights into wireless networks which are briefly summarized in the next section.

III. Summary of Results

We only summarize the results below. The reader is referred to [4] for technical details.

1) **Outerbound :** We provide an outerbound to the degrees of freedom *region* of the $M \times N$ X network. The degrees of freedom *region* outerbound is important since it can be used to

bound for the degrees of freedom of most fully connected distributed one-way single hop network communications scenarios. The outerbound implies that the *total* degrees of freedom of the $M \times N$ X network cannot exceed $\frac{MN}{M+N-1}$.

2) **Achievable Scheme - Interference Alignment :** The outerbound of $\frac{MN}{M+N-1}$ is shown to be tight, if the channel was frequency selective (or time-varying) using an achievable scheme based on interference alignment over multiple-symbol extensions of the channel extensions. Since the outerbound and achievable scheme are tight in the degrees of freedom sense, the capacity of X networks can be characterized as

$$C(\log(\text{SNR})) = \frac{MN}{M+N-1}\log(\text{SNR})+o(\log(\text{SNR}))$$

3) X **networks versus interference networks :** If $M = N = K$ and K is large, the X network has $\frac{K^2}{2K-1} \approx K/2$ degrees of freedom. This implies that there is no significant improvement in high SNR performance in increasing the number of messages of a large interference network to an X network.

4) **Joint versus distributed processing :** If $M \gg N$ or if $N \gg M$, the $M \times N$ X network, much like the MIMO point-to-point channel with M transmit and N receive antennas, has a capacity of $M \times N \log(\text{SNR}) + o(\log(\text{SNR}))$ i.e. it has $\min(M, N)$ degrees of freedom. Thus if $M \gg N$ or $N \gg M$, there is no loss of distributed processing in wireless networks. This observation is an optimistic result from the point of view of wireless networks since it suggests that, under certain conditions, distributed single antenna nodes with no prior common information can obtain the same throughput as the case where they are a single node with multiple antennas.

REFERENCES

[1] V. R. Cadambe and S. A. Jafar, "Interference alignment and degrees of freedom region for the k user interference channel," *arxiv.org*, 2007. arxiv eprint = cs/0707.0323.

[2] S. A. Jafar and S. Shamai, "Degrees of freedom region for the mimo x channel," *arxiv.org*, 2006. arxiv eprint = cs/0607099.

[3] M. A. Maddah-Ali, A. S. Motahari, and A. K. Khandani, "Signaling over mimo multi-base systems: Combination of multi-access and broadcast schemes," *Information Theory, 2006 IEEE International Symposium on*, July 2006.

[4] V. R. Cadambe and S. A. Jafar, "Degrees of freedom of wireless x networks," *arxiv.org*, 2007. arxiv eprint = cs/0711.2824.

CPCC Fellowship Progress Report, Fall 2007:

Space-Time Block Coded Reconfigurable MIMO Communication System Using Practical Antennas

Fatemeh Fazel, Advisor: Hamid Jafarkhani
Center for Pervasive Communications and Computing
EECS, University of California, Irvine
{fazel,hamidj}@uci.edu

I. Project Motivation

By intentionally changing the propagation characteristics of the antenna, one can create additional degrees of freedom in a communication system. The motivation for this project is:

- to introduce block coding schemes that are capable of extracting these additional degrees of freedom offered by employing reconfigurable antennas at the transmitter and the receiver;
- to consider the effects of practical issues associated with the antenna and the channel, therefore, providing a realistic model.

II. Progress Report

First we provide a realistic model of the system. We consider two practical antennas: ORIOL and PIXEL antennas. The ORIOL antenna, is a compact dual-polarized reconfigurable 2-port antenna based on a single octagonal microstrip patch. By exciting the patch from the two points located in perpendicular faces, the ports of the antenna excite two orthogonal polarizations of the radiated electric field. The antenna also has the capability to reconfigure the polarization base in two different radiation states, vertical/horizontal ($0°/90°$) or slant ($\pm 45°$). We include the practical channel measures into our system by defining the Cross Polarization Discrimination (XPD) factor (α_p for state p), transmit and receive correlation factors (t_p and r_p) and the inter channel propagation state correlation matrix ($\mathbf{R}_{12}$), which is a measure of the correlation in between channel propagation states. In [1], we presented an open loop MIMO system using reconfigurable antennas at both the transmitter and the receiver. We showed that the maximum achievable diversity gains in such a scenario are given by the product of the number of transmit and receive antennas and the number of reconfigurable states at the transmitter and the receiver. We were able to show that a system using reconfigurable antennas with P propagation states could benefit from a maximum P-fold increase in the diversity gain over a non-reconfigurable MIMO system. We then analytically derived the diversity gain and the coding gain of the system taking into account the practical concerns. Furthermore, we proposed a coding schemes for an open loop MIMO Reconfigurable system and verified our scheme over the practical case of ORIOL antennas. In addition to the results in [1], we also verified our scheme over another practical antenna called PIXEL and showed that our proposed scheme is capable of demonstrating improved performance. Using ORIOL antennas at both sides of the communication system, we have $M_T = 2$ transmit antennas and $M_R = 2$ receive antennas and $P = 2$ propagation states. We assume that no channel state information is available at the transmitter but the receiver is assumed to have perfect channel knowledge. Without any feedback from the receiver, we employ an alternating scheme, in which the transmitter and receiver ORIOL antennas switch their radiation states periodically, therefore creating a block fading channel. CPS1 and CPS2 represent the two channel state propagations. As we notice from the figure, at a bit-error-rate of 10^{-4}, the performance of the new coding scheme using the realistic reconfigurable ORIOL antenna is about 3 dB better than that of the corresponding non-reconfigurable case. In the ideal system model, the performance improvement is about 4.5 dB.

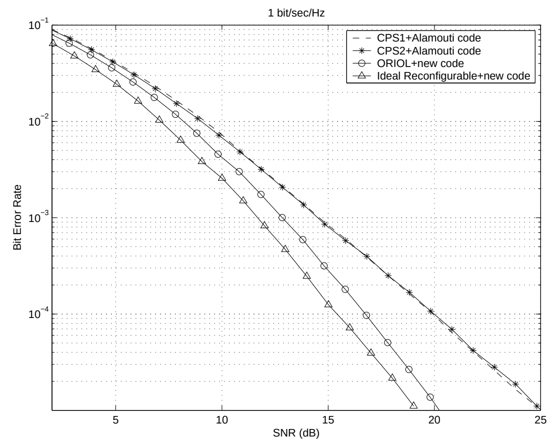

Fig. 1. BER vs. SNR for an ORIOL-based multi-antenna system; BPSK.

References

[1] F. Fazel, A. Grau, H. Jafarkhani and F. De Flaviis, "Space-Time Block Coded Reconfigurable MIMO Communication System Using ORIOL Antennas", *Wireless Communication & Networking Conference* (WCNC) 2008.

Uses and Misuses of Peer-to-Peer Systems

Progress Report for Fall 2007

Student: Minas Gjoka (*mgjoka@uci.edu*)
Advisor: Athina Markopoulou
Center of Pervasive Communications and Computing
University of California, Irvine

***Abstract*— During this quarter, the student studied the use of peer-to-peer systems to support video-on-demand with DVD functionality (i.e. to allow for fast forward and rewind operations). This was a continuation of his summer project during his internship with Telefonica Research, Barcelona. This work involves both (i) system design and implementation and (ii) analytical models to capture the user behavior and analyze the system performance in terms of server capacity and user delay.**

I. Introduction

Video content distribution to a large number of users is gaining momentum on the Internet. Peer-to-peer (P2P) systems are increasingly used to support video, in various modes such as file downloads, live media streaming and video-on-demand (VoD). Supporting advanced DVD-like features, such as backward and forward jumps, is challenging in P2P systems, although these features are quite common in home theaters and online client-server solutions. Supporting a VoD system with advanced features using P2P technologies is challenging because of the lack of synchronization among users, which reduces the segment sharing opportunities. It is desirable to design a system that meets simultaneously the following two requirements: (i) minimize the delay from a user's perspective and (ii) maximize the utilization of the system resources (e.g. server capacity and bandwidth).

In the ideal scenario, the server should only be used if there are not enough peers in the system that can satisfy the demand. However, finding those peers or freeing their resources is non-trivial. In fact, current state-of-the-art approaches for VoD over P2P rely either on over-provisioned servers and/or on structured overlays to quickly find the segments that users request [2]. Another challenge is that the server load heavily depends not only on the system design but also on the arrival pattern of user requests and their viewing preferences. Currently, little is known about how such parameters affect the server requirements.

II. Progress

First, with regards to the server requirements, we studied the impact that jump operations can have on the server load and in the VoD experience. Analytical and experimental results were derived for an array of synthetically generated jumping/viewing patterns (random jumps of various characteristics) and arrival patterns (flash crowd, batch and Poisson arrivals). We also studied the impact of realistic viewing patterns captured from a real, deployed VoD system at Telefonica, in Bareclona, Spain.

Second, we built Kangaroo - a mesh-based P2P system that can efficiently deal with "jumps", i.e. provides users with a high-quality VoD service while requiring only a small capacity at the server. This is achieved by making careful design choices in several aspects of the system. In particular, we included a scheduling policy that combines selfish with altruistic behavior for continuous playback with the goal of improving block diversity. We also included a topology manager that helps peers at similar playback points to mesh with each other and to quickly find peers with the desired data segments during jump operations. From the insight gained from studying the effect of various workloads, we evaluated the performance of Kangaroo and showed that it is close to the best possible. In addition, the system is shown to be scalable for a large number of users. Overal, our preliminary results using realistic jumping patterns showed that Kangaroo can achieve a good user experience without aggressively prefetching or over-provisioning the system, techniques that are common in previous work on this area [2].

III. Future Work

We plan to extend this work in several directions. One possibility is to add new mechanisms which would allow the system to deliver similar performance in a non-collaborative environment. Incentives need to be gracefully tied with the already existing key design mechanisms. Another possibility is the formulation and implementation of an admission control module that allows the server to evaluate/decide the feasibility of supporting the demands of a peer. We also plan to compare the effect of different workloads and jumping patterns on the server load.

References

[1] Xiaoyuan Yang, M.Gjoka, P. Rodriguez, A. Markopoulou"Understanding the impact of VCR operations in P2P VoD systems", *work in progress*.

[2] N. Vratonjic, P. Gupta, N. Knezevic, D. Kostic, A. Rowstron, "Enabling DVD-like features in P2P Video-on-Demand Systems," *in Proc. of ACM P2P-TV SIGCOMM Workshop 2007.*

Progress Report on Multiple-Antenna Front-End Design Research: Fall 2007

Amin Jahanian Advisor: Payam Heydari
Nanoscale Communications Integrated Circuits Lab
Center for Pervasive Communications and Computing
Department of Electrical Engineering and Computer Science
The Henry Samueli School of Engineering
University of California, Irvine, CA 92697-2625
Email: jahanian@uci.edu

***Abstract* — In the Fall quarter, we tested a previously fabricated chip in which a novel 5GHz multi-antenna RF front-end, capable of performing spatial multiplexing, spatial diversity, and beamforming was implemented. In the designed receiver front-end architecture, the use of a unique code-modulation scheme at the RF stages of the signal paths enables linear combination of all mutually orthogonal code-modulated received signals. The combined signal is then fed to a single RF/baseband/ADC chain, resulting in a significant reduction of power consumption and area, as well as mitigating the issue of LO routing/distribution. In the digital domain, all antenna signals are fully recovered.**

I. Introduction

Multi-antenna communications promises higher data rates using spatial multiplexing (SM), and increased range using spatial diversity (SD) and beamforming (BF). The use of multiple antennas in any MIMO RX may entail multiple RF chains, baseband blocks and ADCs [1], [2]. Consequently, there will be considerable increase in power consumption and chip area. In addition, having multiple receive chains results in a complicated LO routing and distribution task.

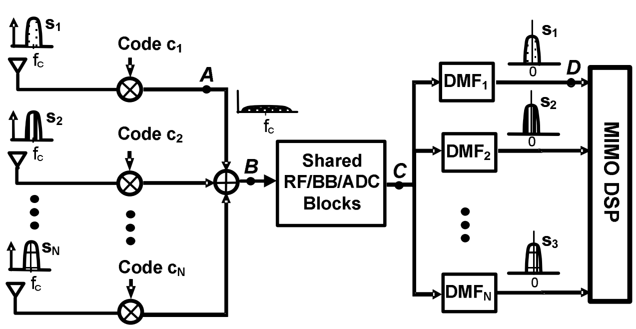

Fig. 1. Conceptual diagram of the proposed CPMA receiver

Previously in this project, we had presented a new **code-modulated path-sharing multi-antenna** (CPMA) RX front-end architecture that enables sharing of RF, baseband, and ADC blocks among multi-antenna signals. The underlying idea is to implement a code modulation system *within* the multi-antenna RX in order to distinguish antenna signals before combining them in the RF domain. More specifically, *N* antenna signals are modulated by *N* orthogonal code sequences. The mutual orthogonality of code-modulated signals allows signal combination in the RF domain, while promising full recovery of each signal in the baseband using digital matched filters (DMF). The recovered signal is then fed to the MIMO DSP for further processing. The proposed CPMA RX front-end is capable of accommodating any multi-antenna scheme, including SM, SD (including OSTBC, MRC, and BF). The advantages of this architecture include significant reduction of power consumption and chip area, and mitigation of coupling between antenna signals in the RX. Moreover, the single path alleviates the problem of LO distribution and routing in multi-antenna architectures.

The proposed CPMA architecture has been implemented for the special case of a 5GHz two-antenna super-heterodyne receiver consisting of LNA, mixers, baseband LPFs, and VGAs, as depicted in Fig. 2.

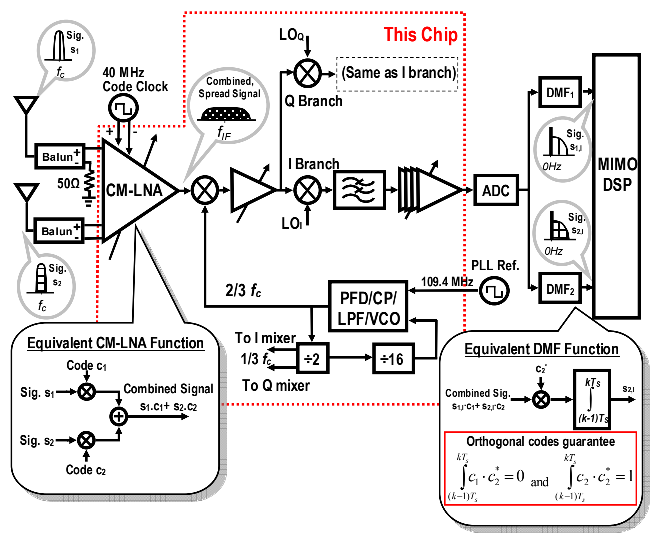

Fig. 2. Implemented dual-antenna super-heterodyne CPMA receiver IC

II. Implementation And Measurement Results

To demonstrate the principle, a prototype receiver (Fig. 3(a)) was designed and fabricated in 0.18μm CMOS. In the Fall quarter, the CPMA RX functionality was verified using the test setup in Fig. 3(b). Two independent data symbols, sym_1 and sym_2, are generated and transmitted through a 2×2 MIMO channel, and sent to an arbitrary waveform generator. All signals are upconverted and input to the CPMA chip. I/Q outputs are digitized by an oscilloscope, functioning as the ADC. Each signal is recovered by its designated DMF to be decoded by the MIMO detector.

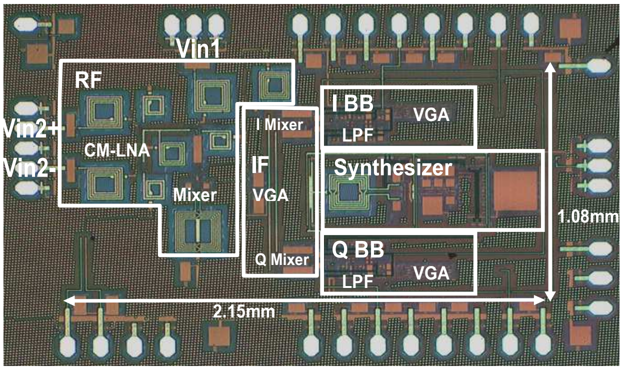

(a)

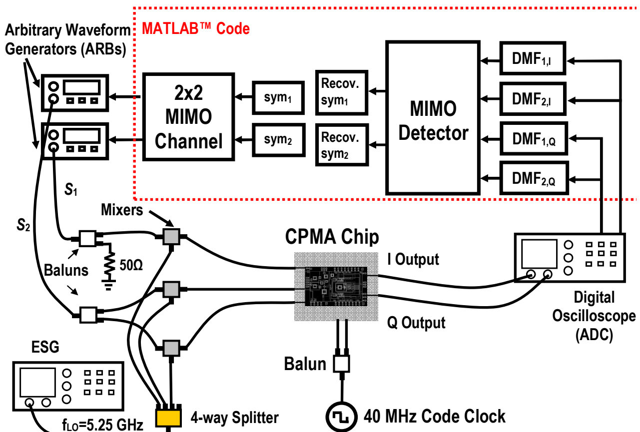

(b)

Fig. 3. (a) CPMA receiver die photo, and (b) Test setup for data acquisition.

Measurements were carried out for three 2×2 multi-antenna schemes, namely SM, SD, and BF, and corresponding symbol error rates (SER) were plotted against the average input power (Fig. 4). The uncoded SM scheme used a minimum mean square error detector to separate original symbols. The SD employed orthogonal space-time block codes [3] and a maximum likelihood detector. The BF used optimum transmit/receive weights chosen from [4] to perform MRC. In Fig. 4, the slopes of the SER curves will be approximately constant for input powers greater than or equal to −75, −78, and −80 dBm, for SM, SD, and BF, respectively, because of higher SNR. At these input power ranges, the slopes for the SD and BF curves are approximately 4 times that of SM, highlighting their diversity gain. The BF curve shows a left-hand shift of approximately 2 dB with respect to the SD curve, which is the result of antenna gain. Thus, the CPMA receiver exemplifies measurements that conform with theory, proving that it is capable of realizing different multi-antenna schemes.

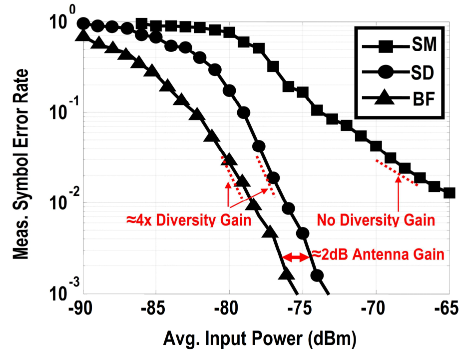

Fig. 4. SER vs. average input power for SM, SD, and BF

The prototype occupies only 2.31 mm^2 and the standalone RX chain consumes only 47mW of power, emphasizing the advantages of path-sharing. The measured closed loop output phase noise of the frequency synthesizer shows a phase noise of $-109 dBc/Hz$ at $1 MHz$ offset.

References

[1] A. Behzad, *et al*, "A fully integrated MIMO multi-band direct-conversion CMOS transceiver for WLAN applications (802.11n)," *ISSCC Proc.*, pp. 560-561, Feb., 2007.

[2] Y. Palaskas, *et al*, "A 5-GHz 108-Mb/s 2x2 MIMO transceiver RFIC with fully integrated 20.5-dBm P_{1dB} power amplifiers in 90-nm CMOS," *IEEE J. Solid-State Circuits*, vol. 41, no. 12, pp. 2746-2756, Dec. 2006.

[3] V. Tarokh, H. Jafarkhani, and A. Calderbank, "Space-time block codes from orthogonal designs," *IEEE Trans. Inform. Theory*, vol 45, no. 7, pp. 1456-1467, July 1999

[4] T.K.Y. Lo, "Maximum ratio transmission," *IEEE Trans. Comm.*, vol. 47, no. 10, pp. 1458-1461, Oct. 1999.

UC Irvine Center For Pervasive Communications and Computing Graduate Fellowship Progress Report Fall 2007

February 19, 2008

Project Name: Adaptive Equalization of Multimode Fiber Channels in $0.13\mu m$ CMOS
CPCC Affiliate Professor: Michael Green
Mailing Address: 544 Engineering Tower, Irvine CA 92697-2625
Phone No.: 949-824-1656 **E-mail:** mgreen@uci.edu
Student Fellowship Recipient: Mahyar Kargar

Introduction

With increasing data rates and link distance in fiber-optic systems, the transmission path becomes severely limited by fiber non-idealities, especially dispersion. Intersymbol interference (ISI) is a fundamental limiting factor in band-limited communication links. In particular, in multimode optical fiber, which are the dominant fiber type in local area network (LAN) links like 10Gb/s Ethernet,the ISI is mainly due to modal dispersion. Electronic dispersion compensation (EDC) is used to combat this ISI in short-distance fiber links. Use of adaptive equalizers as an EDC method is known to make the data communications over short ranges of the MMF possible. In this project a high-speed adaptive DFE is designed to combat the ISI caused by the band-limited MMF channel.

Summary of Accomplishments

The design of feed-forward filter (including the DLL and gain control loop) and the adaptive feedback filter (including high-speed slicer and DFF's) has been completed in $0.13\mu m$ CMOS. LMS algorithm is implemented using an analog integrator and a Gilbert multiplier.

The project is in the layout and integration mode now. The building blocks of the feed-forward and feedback filters have been laid out and the results have been verified with post-layout simulations. The 10Gb/s CDR design is almost completed.

A 10GHz LC VCO with ± 10% tuning range is realized to be used in the CDR loop. The VCO layout has been completed and verified. The VCO tuning range and phase noise after post-layout simulations are shown in Fig. 1(a) and 1(b), respectively. The tuning range is from 9.09GHz to 10.98GHz. The phase noise is -101.5dBc/Hz at 1MHz offset.

Ongoing Work

1. Verification of the feed-forward filter with post-layout simulations on extracted blocks after layout.
2. Verification of the feedback filter with post-layout simulations extracted blocks after layout.
3. Verification LMS circuit convergence properties using transistor level post-layout simulations.
4. Design of a 10Gb/s Alexander phase detector for the binary CDR.
5. Top level simulation of the 10Gb/s CDR verifying the locking behavior and performance.
6. Layout and post-layout extraction of the remaining blocks in the CDR.

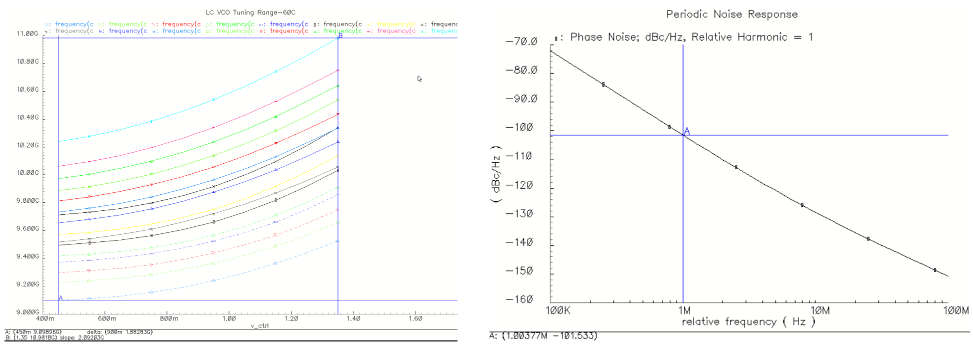

(a) (b)

Figure 1: 10GHz LC VCO(a)Tuning range (b) Phase noise

Progress Report on Aggressive Power Management Utilizing Fault Tolerant Adaptation for Wireless Systems: Fall 2007

Amin Khajeh Djahromi, Advisor: Professor Ahmed Eltawil
Center for Pervasive Communications and Computing
Department of Electrical Engineering and Computer Science
The Henry Samueli School of Engineering
University of California, Irvine
Irvine, California 92697-2625
Email: akhajehd@uci.edu

***Abstract*—This report presents a new approach of utilizing body biasing in order reduce failures in 6T-SRAM due to aggressive voltage scaling. The SRAM failure is simulated for three different cases: 1) reverse body bias, 2) zero body bias and, 3) forward body bias.**

I. Introduction

For the past decade researchers have used body biasing to shift the threshold voltage of MOSFET devices to a desired value. For example Roy in [7] uses an adaptive scheme that adaptively changes the body bias in order to reduce the effect of the inter-die V_{th} variation by shifting the average threshold of the devices on the chip to a nominal value and therefore resulting in higher yield in the Static Random-Access Memories (SRAM). Also Blaauw in [8] has examined an energy reduction technique through simultaneous implementation of dynamic voltage scaling (DVS) and adaptive body biasing (ABB) and presented an analytical expression for power consumption and processor performance.

In the absence of process variation, the threshold voltage is a fixed number and any changes in the body bias voltage, V_{SB}, affects the value of the threshold voltage, V_{th}. However, in the presence of process variation, V_{th} will follow a distribution which is conventionally assumed to be Gaussian [1]. This Gaussian distribution of V_{th} has a mean $\mu_{V_{th}} = V_{th0}$ and standard deviation which can be calculated as[13]:

$$\sigma_{V_{th}} = \sigma_{V_{th0}} * \sqrt{\frac{L_{min}}{L}\frac{W_{min}}{W}} \tag{1}$$

where $\sigma_{V_{th0}}$ is the $\sigma_{V_{th}}$ for minimum sized transistor and it is given by[14]:

$$\sigma_{V_{th0}} = \frac{qT_{ox}}{\varepsilon_{ox}} * \sqrt{\frac{N_a W_d}{3L_{min} W_{min}}} \tag{2}$$

where W_d is the depletion region width, T_{ox} is the oxide thickness, L_{min} and W_{min} are the minimum channel length and width respectively. It is important to note that this model is true only for zero body biasing. Traditionally the assumption is that by applying the body bias, only the mean of the V_{th} changes and the shape of the V_{th} distribution remains the same. In other words any change in V_{SB} only changes the $\mu_{V_{th}}$ and $\sigma_{V_{th}}$ remains untouched. This assumption may be true for technologies where the process variability is negligible, however in this work we will study the impact of process variation in highly scaled technologies on the threshold voltage distribution. The reminder of this report is organized as follows. In section II we study the effect of the body biasing on the threshold voltage distribution while considering random dopant fluctuation. Section III discusses the effect of body biasing on SRAM stability.

II. Effect of Body Biasing on Threshold Voltage

As mentioned in the previous section, body biasing changes the distribution of the threshold voltage in MOSFET devices. In this work we only consider the effect of random dopant fluctuations (RDF) on the threshold voltage variation since RDF has the maximum effect of the threshold voltage. Figure 1 illustrates that along with the technology scaling, the number of the atoms in the channel reduces. While it is possible to control the average number of the atoms in the channel, N_{avg} , it is almost impossible to assign the exact same number of atoms to each device. In fact, the number of the atoms in the channel, N, follows a Poisson distribution as the follows:

$$f(N; N_{avg}) = \frac{N_{avg}{}^{N_a} e^{-N_{avg}}}{N!} \tag{3}$$

This variation in the number of the atoms in the channel will cause variation in the threshold voltage.

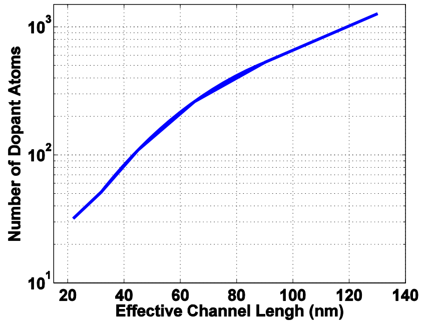

Figure 1: Number of doping atoms in the channel[9]

In order to study the effect of the body biasing on the threshold voltage distribution, V_{th} of MOSFET transistors can be modeled as [2]:

$$V_{th} = V_{FB} + 2\phi_F + \frac{\sqrt{2\varepsilon_{si} q N_a (2\phi_F + V_{SB})}}{C_{ox}} \qquad (4)$$

where V_{FB} is the flat band voltage, ε_{si} is permittivity of silicon, q is the electron charge, N_a is the substrate doping concentration, C_{ox} is the capacitance per unit area presented by the gate oxide and ϕ_F can be calculated from:

$$\phi_F = V_t * ln\frac{N_a}{n_i} \qquad (5)$$

where n_i is the intrinsic carrier concentration of silicon and V_t is the thermal voltage. For each technology node we will have:

$$N_a = N_0 * N \qquad (6)$$

where N can be picked from a Poisson distribution given by equation 3. By replacing the N_a from equation 6 into equation 4, we can find the distribution of threshold voltage as a function of body bias. Figure 2 shows the effect of the body biasing on the mean of the threshold voltage. As expected, forward body bias (FBB) reduces the mean of the threshold voltage and reverse body bias (RBB) increases the mean of the threshold voltage. Figure 3 illustrate the effect of the body biasing on the standard deviation of the threshold voltage. Unlike the traditional assumption that body biasing does not change the standard deviation of the threshold voltage, our result shows that FBB reduces the $\sigma_{V_{th}}$ and RBB increases $\sigma_{V_{th}}$.

Authors in [5] have shown that aggressive voltage scaling can be used to reduce power consumption in wireless and multimedia systems. The fault adaptation technique utilizes the available slack and redundancy in such system to allow limited and controllable amount error in the memories which are identified as fault tolerant memories. This technique reduces the supply voltage of the fault tolerant memories beyond the safe operating point and compensate for the resulting errors at the system level which results in considerable savings in both dynamic and leakage power. In the following section we will show that an adaptive body biasing technique can be used jointly with aggressive voltage scaling in order to reduce memory failures at lower voltages.

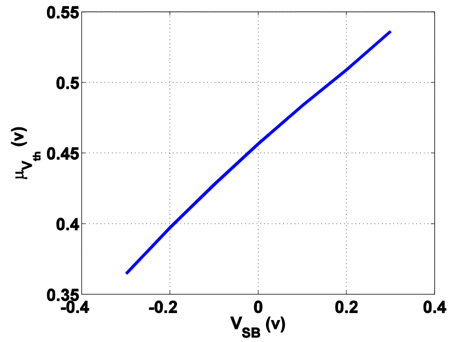

Figure 2: Effect of body biasing on the mean of threshold voltage.

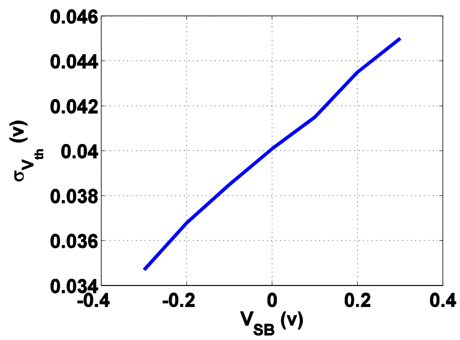

Figure 3: Effect of body biasing on the standard deviation of threshold voltage.

III. Effect of Body Biasing on SRAM Satiability

Figure 4 shows the typical six-transistor cell used for CMOS Static Random-Access Memories (SRAM). The cell consists of two cross-coupled CMOS inverters (*NL-PL* and *NR-PR*) that store one bit of information, and two N-type transistors(*SL* and *SR*) that connect the cell to the bitlines (*BLC* and *BLT*).

Since the placement and the number of dopants in the channel of one transistor depend only on the geometry of that transistor and are independent of the placement and number of dopants in the channel of neighboring transistors, the V_{th} fluctuation due to RDF, $\Delta_{V_{th}}$, of one transistor does not depend on V_{th} fluctuation of any neighboring transistor. Hence $\Delta_{V_{th}}$ of the cell transistors can be assumed as independent random variables with zero mean and standard deviation of $\sigma_{V_{th}}$ [2]. The standard deviation of the $\Delta_{V_{th}}$ due to RDF, $\sigma_{V_{th}}$, depends on the manufacturing process, doping profile, transistor sizing and body bias value.

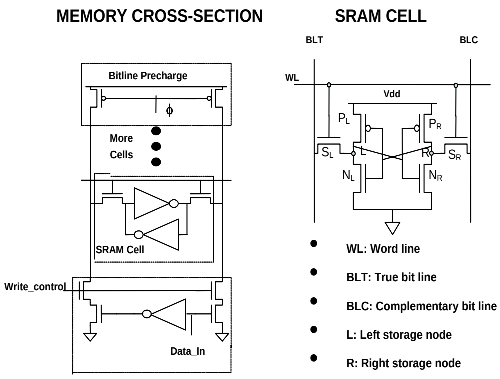

Figure 4: 6T SRAM cell

Now we will consider the effect of body bias (only on NMOSs, S_L , S_R , N_L and N_R) on the SRAM cell failures.

Applying reverse body bias (RBB) increases both $\mu_{V_{th}}$ and $\sigma_{V_{th}}$ of the transistors. Increase in $\mu_{V_{th}}$ results in slower transistors and therefore it increases the read access time failure and write failure. An increase in $\sigma_{V_{th}}$ results in higher mismatch between transistors which leads to further increase in the read access and write failures. Furthermore, increase in $\mu_{V_{th}}$ reduces the read voltage (V_{read} which is the voltage at node L(R) while reading '0' ('1') from the cell) which results in reduction in destructive read failure. However, since the variation of the threshold voltages, $\sigma_{V_{th}}$, have increased, the destructive read failure will be still higher than that of the case with smaller $\sigma_{V_{th}}$.

Applying forward body biasing (FBB) reduces $\mu_{V_{th}}$ and $\sigma_{V_{th}}$of the transistors which results in faster transistors and therefore it reduces the read access time failure and write failure. Reduction of $\sigma_{V_{th}}$ results in fewer mismatches between transistors which leads into even lower read access and write failures. In addition, reduction of $\mu_{V_{th}}$ increases V_{read} which results in an increase in destructive read failure. However, since the variation of the threshold voltages, $\sigma_{V_{th}}$, have been reduced, the destructive read failure will be lower than that of the case with higher $\sigma_{V_{th}}$.

Figure 5 shows the effect of FBB and RBB on the overall failure of SRAM cell. These failures are calculated based of our previous work. This figure shows that by applying FBB we can reduce the probability of failure at aggressively scaled voltages.

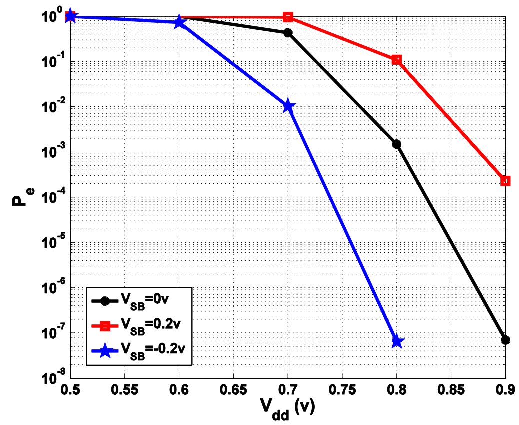

Figure 5: Effect of body biasing on the standard deviation of threshold voltage.

IV. References

[1] Y. Taur and T. H. Ning "Fundamentals of Modern VLSI Devices" Cambridge University Press 1998.

[2] A. Bhavnagarwala, X. Tang and J. D. Meindl. "The impact of intrinsic device fluctuations on cmos sram cell stability". JSSC , April 2001.

[3] www-device.eecs.berkeley.edu/~bsim3/bsim4_intro.html

[4] Calhoun, B. H., A. Wang, A. Chandrakasan, "Modeling and Sizing for Minimum Energy Operation in Subthreshold Circuits," IEEE JSSC, vol. 40, no. 9, September 2005.

[5] Amin Khajeh Djahromi, Ahmed M. Eltawil, Fadi Kurdahi and Rouwaida Kanj, UC Irvine and IBM "Cross Layer Error Exploitation for Aggressive Voltage Scaling" 2007

[6] Amin Khajeh Djahromi, Ahmed M. Eltawil, and Fadi Kurdahi "Fault Tolerant Approaches Targeting Ultra Low Power Communications System Design," VTC 2007.

[7] S. Mukhopadhyay, K.Kim,H. Mahmoodi,K. Roy, "Design of a Process Variation Tolerant Self-Repairing SRAM for Yield Enhancement in Nanoscaled CMOS," JSSC, Vol 42, NO.6, June 2007.

[8] S. M Martin, K. Flautner, T. Mudge, D. Blaauw, "Combined Dynamic Voltage Scaling and Adaptive Body Biasing for Lower Power Microprocessors under Dynamic Workloads," ICCAD, November, 2002

[9] D.J. Frank, R.H. Dennard,E. Nowak,P.M. Solomon,Y Taur, Hon-Sum Philip Wong, "Device scaling limits of Si MOSFETs and their application dependencies," Proceedings of the IEEE , vol.89, no.3, pp.259-288, Mar 2001

[10] V. Gutnik and A. Chandrakasan, "Embedded power supply for lowpower DSP," IEEE Trans. VLSI Syst., vol. 5, no. 4, pp. 425–435, Dec. 1997.

[11] B. H. Calhoun, A. P. Chandrakasan, "Ultra-Dynamic Voltage Scaling (UDVS) Using Sub-Threshold Operation and Local Voltage Dithering" IEEE JSSC Vol. 41, No. 1, Jan. 2006.

[12] The International Technology Roadmap for Semiconductors (ITRS) http://www.itrs.net/Links/2005ITRS/Home2005.htm

[13] H. Mahmoodi, S. Mukhopadhyay and K. Roy. "Modeling of failure probability and statistical design of sram array for yield enhancement in nano-scaled cmos". IEEE TCAD , *2003*

[14] S. Mukhopadhyay, H. Mahmoodi, and K. Roy "Statistical Design and Optimization of SRAM Cell for Yield Enhancement," ICCAD 2004

Power-Aware Interconnection Network for Wireless Mobile Systems: FALL 2007

Seung Eun Lee, Advisor: Nader Bagherzadeh
Center for Pervasive Communications and Computing
University of California-Irvine
Email: seunglee@uci.edu

***Abstract*—In our earlier work, we proposed the clock boosting mechanism. In Fall 2007, we extended the mechanism to a variable frequency link for a power-aware interconnection network and applied a dynamic frequency scaling (DFS) policy to the link, that judiciously adjusts link frequency based on link traffic. Experimental result shows that history-based DFS successfully adjusts link frequency to track actual link utilization over time.**

I. Introduction

In Fall 2007, we extended the clock boosting mechanism [1] to a variable frequency link for a power-aware interconnection network and applied a dynamic frequency scaling (DFS) policy to the link. The clock boosting router provides a variable frequency link that is applicable for DFS with negligible hardware cost and fast response time to frequency changes. In addition, the operating frequency of a system is not limited by the critical path of the route decision logic because it only changes clock frequency for the body it transmission. Thus, it not only provides variable frequency link but also increases interconnection network performance. Also, fast response time of the clock domain variations make it possible to use narrow control period for the DFS control, adjusting the clock frequency in more frequently. A history based DFS policy was implemented and applied to the proposed DFS link, demonstrating the power saving in an on-chip interconnection network.

II. History-based DFS

The history-based DFS policy was applied to the DFS link. The threshold values for the link controllers, π_u and π_l, were set to 80% and 50%, respectively.

Figure 1 shows the simulation result of the history-based DFS policy when the control period (T_c) is 8 cycles. Link utilization estimator predicts future workload based on the history of workload (Fig. 1(b)). The DFS policy dynamically adjusts the link frequency according to the link utilization level (Fig. 1(c)). Figure1(d) shows that history based DFS successfully adjusts link frequency to track actual link utilization over time, reducing dynamic power consumption for an interconnection network. Figure 1(e) presents latency for each flit. It proves that the history based DFS policy reduces latency with the expense of more power consumption per link. For instance, under the heavy traffic load (marked as "A") link utilization level as well as latency increase, reducing throughput of the link. By applying DFS, the link controller changes the boosting frequency from 1x to 4x, consequently reducing latency at the expense of more power consumption. When link utilization level goes low because of the reduced workload, link controller decreases the boosting frequency, reducing power consumption.

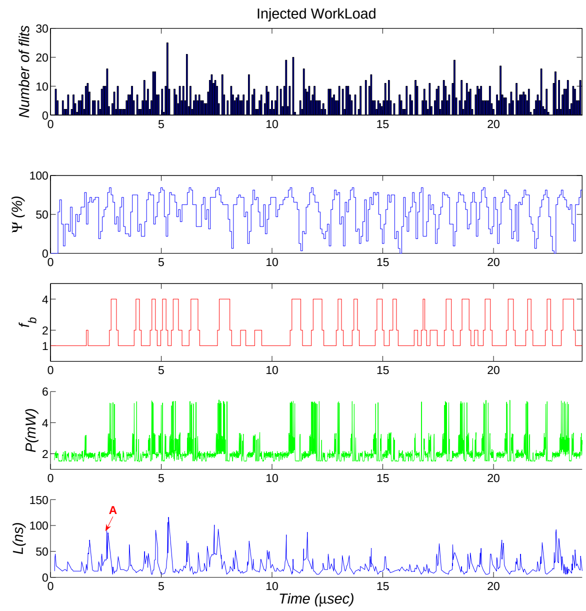

Fig. 1. Simulation result of the history-based DFS policy when T_c is 8 cycle. (a) injected workload, (b) Ψ_L: link utilization estimation, (c) f_b: state of boosting clock (1x, 2x, and 4x), (d) P: power consumption, and (e) L: latency for each flit.

A wider control period further slows down the adaptation of link frequency for the given traffic, exacerbating latency. While there is trade off in power and performance for the control period from 8 to 64 cycles, the history-based DFS with 128 control periods consumes more power but also increases the latency because of selecting a long control period for the given workload.

References

[1] S. E. Lee and N. Bagherzadeh, "Increasing the throughput of an adaptive router in network-on-chip (noc)," in *CODES+ISSS'06: Proceedings of the 4th international conference on Hardware/software codesign and system synthesis*, 2006, pp. 82–87.

Progress Report on Fault Tolerant Techniques to Mitigate Process Variation

Mohammad A Makhzan
Advisors: Fadi Kurdahi and Ahmed Eltawil.
Center for Pervasive Communications and computing
Department of Electrical Engineering and Computer Science
The Henry Samueli School of Engineering
University of California Irvine
Irvine, California 92697-2625
Email: mmakhzan@uci.edu

Abstract- As the technology migrates to smaller geometries, parametric Process Variation tends to be of a bigger concern since it severely affects the operation of both logic and memory in an embedded system. Process variation's importance in a voltage scalable system is further increased since as the operating voltage is decreased towards the threshold voltage, smaller variations could also result in a logic or memory operation failure. Our laboratory (and my academic) focus is on designing Fault Tolerant systems that the effect of process variation is mitigated either in circuit or in the system level.

Introduction:

We focused our efforts into two different system structures.

1- Systems that are inherently (totally or partially) fault tolerant.
2- Systems which are not tolerant to faults.

Multimedia and wireless application could be categorized in the first category where the Control Unit, some caches, register files and … could be categorized in the second. Usually systems in the first category are designed to deal with human receptors and since the sensitivity of human receptors is not very high, small variation in system output as far as it is close enough to the original output, are not noticeable to the naked human receptor. In such cases when designing a system, 100% correctness is not a necessity. In the second case the design space is more restricted and correctness requirements are enforced. For this category a fault tolerance architecture should be able to detect and cover 100% of the defects and the output of the system should be no different than a system with no defect.

As an example of the first category we choose the JPEG2000 as our working architecture. In this architecture we lowered the voltage in the embedded memory of JPEG2000 and analyzed how defects are generated and how the image quality is affected by memory defects. Study of the artifacts resulted from coefficient corruption (in the result of saving the coefficients in the SRAM memory of system) revealed that defects due to the specific encoding and compression mechanism used produce a recognizable error pattern. This became a motivation for developing a detection algorithm. We later developed a correction algorithm which in few iterations a decoder could detect and correct the majority of defects in the image and produce a high quality image unrecognizable from the original image. We then planted the detection and correction algorithm in an encoder and coupled a voltage scalable decoder with an iterative fault tolerant decoder. The voltage on the encoder is reduced to increase the battery life. Reducing the voltage increase the number of memory faults and therefore the quality of the image is reduced. The image data is then sent from a media (wireless or internet) to the decoder. We Assumed that the receiver is not portable (doesn't have low power consumption requirements for voltage scaling). After receiving the image data few iteration, the decoder detect and correct most of the defects and produce a reasonable output image. Using this configuration portable encoder could operate at very low voltages where the burden of fault detection and correction is posted to the decoder. In addition as the marriage between a decoder and an encoder continues, the decoder could detect all the errors in the image with only one iteration because in the first few iteration all the defective locations the memory of encoder will be recognized. This work is submitted as a journal paper to TVLSI

A register file or an instruction or data cache (especially if it is exclusive) is a good example of a system or sub-system that is not tolerant to any defects. As stated previously any fault in this system should be covered otherwise the system is not operable. As a case study we worked on an L1 cache in 32nm technology. We studies the effects of process variation on the operation of cache memory cells and its decoder logic. A fault tolerant system based on word level remapping (rather than row level remapping in tradition cache) was developed to increase the coverage of the available redundancy space. In addition the system was designed to be voltage scalable. Based on the voltage level the fault tolerant circuit dynamically configures a new defect mapping layout and all the defects are remapped to the new healthy locations. This study along with an analysis on the power consumption of this structure was submitted to DAC as a conference paper.

Wireless Video Transmission: A Distortion-Optimal Approach

Negar Nejati, Advisors: Hamid Jafarkhani, Homayoun Yousefi'zadeh
Center for Pervasive Communications and Computing
Department of Electrical Engineering and Computer Science
The Henry Samueli School of Engineering
University of California, Irvine
Irvine, California 92697-2625
Email: nnejati@uci.edu

***Abstract*-We identify an analytical expression for the distortion of a scalable video bitstream. Relying on the distortion expression, we propose a low complexity distortion-optimal Unequal Error Protection (UEP) method for the transmission of such video bitstream over wireless tandem channels. Utilizing a one-dimensional Forward Error Correction (FEC) coding scheme, our proposed transmission method protects the bitstream against both bit errors caused by fading and packet erasures caused by network buffering.**

I. INTRODUCTION

In the past decade, multimedia streaming and broadcasting over wireless channels and networks has received a great deal of attention. Despite improvements in wireless network infrastructure, many challenges still exist in providing an acceptable level of Quality of Service (QoS) for video transmission over a wireless channel. We introduce an analytical distortion model for a progressive video stream intended for transmission over a tandem channel. Fig.1 illustrates a sample result of our experiments for Foreman and Grandma sequences.

Utilizing our distortion model and MoMuSys video code implementing MPEG4 standard [2] with fine grain scalability, we formulated and solved a distortion-optimal problem of video transmission over such tandem channel. We proposed a one-dimensional optimized RS code to protect the video bitstream against both bit errors and packet erasures.

We compared the performance of our proposed distortion-optimal method, O1D, with two UEP methods utilizing two dimensional product codes named S2D1[3][8] and S2D2 [3][8] as well as an optimal EEP method called SEEP. S2D1 protects the source symbols unequally against bit errors while packets are protected equally against erasures. S2D2 protects the bitstream against bit errors equally while using unequal protection against the packet erasures and SEEP protects the data block equally against both bit errors and packet erasures. The simulation results are provided in the next section.

II. SIMULATION RESULTS

We provide the results of comparing S2D1, S2D2, SEEP, and O1D methods. In our experiments, we use a tandem channel introducing both bit errors and packet erasures. To capture the effects of bit errors and packet erasures in our study, we have used a two state Gilbert-Elliott (GE) Markov chain and another independent Gilbert (G) Markov chain [5]. We apply transition probabilities of γ=0.99875 and β=0.875 for the GE chain used for bit errors. The average burst lengths associated with these values are 800 and 8, respectively. We choose an SNR range of [4,60]dB for GOOD state of the GE chain and set SNRG=10 SNRB to differentiate between the two states. The G chain used for packet erasures has the same γ as the GE chain and its β parameter changes in the range of [0.87625,0.995]. The results for two different choices of total transmission budget applied to the EL bitstream of Foreman sequence in qcif format are presented in Fig.2. In Fig.2 (a) the total budget for transmitting the EL bitstream is 150% of the size of EL bitstream, the packet size is 20 bytes. As is shown in this figure, our proposed O1D method outperforms the other two product codes, S2D1 and S2D2, and all three methods outperform SEEP especially for small values of SNRG. In Fig.2 (b) the total budget allocated for transmitting the EL bitstream is reduced to 130% of the size of the EL bitstream. In this case we have assumed that the lengths of packets are 40 bytes. The results for Grandma sequence are presented in Fig.3. Again these results show that O1D method outperforms the other methods even with a lower transmission budget.

REFERENCES

[1] P. A. Chou and Z. Miao, "Rate-distortion optimized streaming of packetized media," *IEEE Trans. on Multimedia*, Apr 2006.
[2] "MPEG–4 fine granular scalability verification model version 4.0," *ISO/IEC/JTC1/SC29/WG11/ N3317*, 2000.
[3] F. Etemadi, H. Yousefi'zadeh, and H. Jafarkhani, "A linear-complexity distortion optimal scheme for transmission of progressive packetized bitstreams," *IEEE Sig. Proc. Letters*, May 2005.
[4] F. Etemadi and H. Jafarkhani, "An efficient progressive bitstream transmission system for hybrid channels with memory," *IEEE Trans. on Multimedia*, 2006.
[5] H. Yousefi'zadeh, F. Etemadi, and H. Jafarkhani, "Distortion-optimal transmission of progressive images over channels with random bit errors and packet erasures," *In Proc. DCC*, 2004.
[6] H. Yousefi'zadeh, H. Jafarkhani, and M. Moshfeghi, "Power optimization of wireless media systems with spacetime block codes," *IEEE Trans. Image Processing*, Jul 2004.
[7] P. Cuetos and K. W. Ross, "Unified framework for optimal video streaming," *In Proc. INFOCOM*, 2004.
[8] F. Etemadi, H. Yousefi'zadeh, and H. Jafarkhani, "Progressive bitstream transmission over tandem channels," *In Proc. ICIP*, 2005.

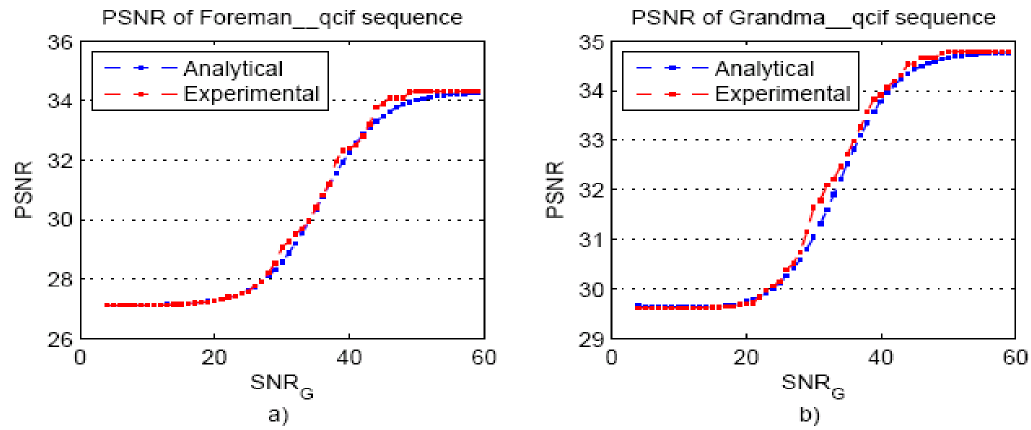

Fig.1 Comparison of analytical and experimental distortion results of
a)Foreman sequence and b)Grandma sequence

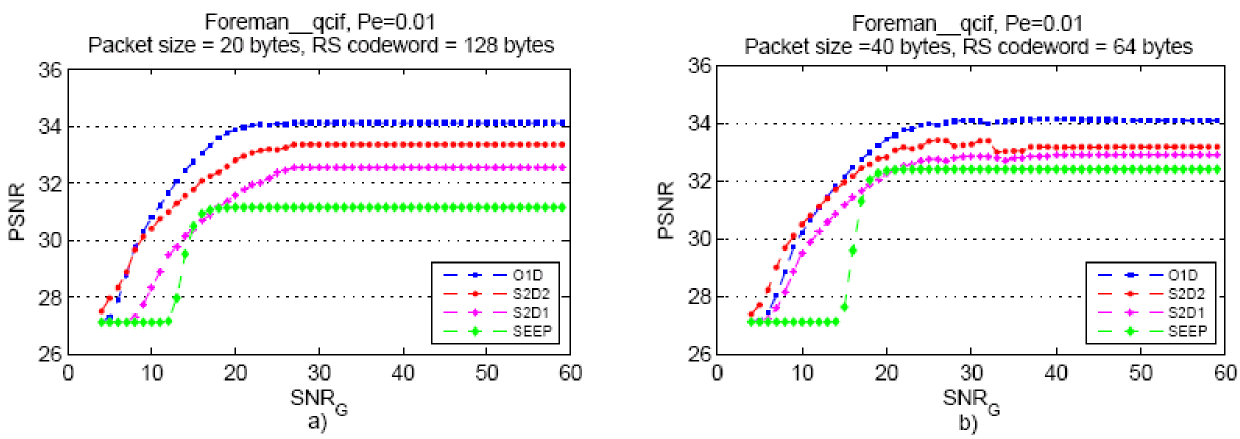

Fig.2 Comparison results of Foreman sequence for a total budget equaling
a) 150% and b) 130% of the size of the original bitstream

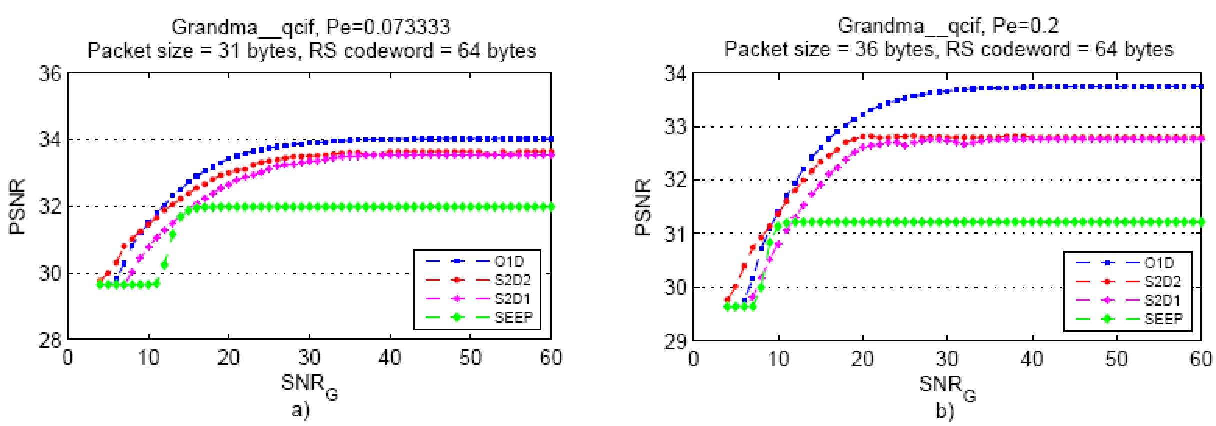

Fig.3 Comparison results of Grandma sequence for a total budget equaling
a)150% and b) 130% of the size of the original bitstream

UC IRVINE CENTER FOR PERVASIVE COMMUNICATIONS AND COMPUTING
Graduate Fellowship - Progress Report for Fall 2007

Project: Network Coding for Video Streaming over Wireless
Ph.D. Student: Hulya Seferoglu
CPCC Affiliate Professor: Athina Markopoulou

During 2006-2007 we developed video-aware opportunistic network coding schemes that improve the quality of video streaming over wireless networks [1]. During the Fall quarter 2007, we continued and completed this work. In particular, the student (i) presented the paper in the Packet Video Workshop 2007 [1] (ii) passed her Qualifying examination and (iii) prepared a journal version, currently under submission to the IEEE Transactions on Multimedia.

For the journal version, the work had to be significantly extended in the following two directions.

1. Evaluation in the GlomoSim Simulation Environment:

We implemented network coding functionality in the GlomoSim Simulation environment [2], as well as our own algorithms, NCV and NCVD. The purpose was to evaluate our algorithms in a realistic environment that takes into account realistic physical and MAC layers, their interactions and also various overheads. This is an improvement over our original work, where the simulations were conducted in our own in-house simulator, which did not address these issues and did not scale for general topologies and large number of nodes. We repeated all simulations in the new environment.

Furthermore, the flexibility of GlomoSim allowed us to consider new topologies, in addition to the one-hop downlink transmission, including the one-hop cross topology and the multi-hop grid topology. In all scenarios, we considered a large number of nodes, while previously we had only considered a toy topology with 3 nodes.

2. Improved Baseline Algorithms:

We also considered and implemented an additional baseline algorithm for comparison, the "Multimedia Streaming Algorithm (MM)", which does rate distortion optimized packet scheduling and error protection as proposed in [4]. This is in addition to the network coding algorithms [3] considered as baseline in our original paper [1]. This addresses one of the comments that came up during the student's Qualifying exam: for a fair evaluation of the benefit brought by our NCV (network coding + video aware) approach, we need to compare it not only to the best network coding-based [3] but also to state-of-the art video-oriented approaches [4].

In addition, we considered an improved NC-based baseline algorithm which we call NCTD: "network coding for throughput, in depth", which is similar to NCT [2] in that it optimizes throughput, and similar to our own NCVD in that it considers all packets in the queue as candidates for primary packets. This provides a fair comparison to the state-of the art NC-based schemes.

With these extensions, this chapter of the work is now complete.

References:

[1] H. Seferoglu, A. Markopoulou, "Opportunistic Network Coding for Video Streaming over Wireless," *in Proc. of Packet Video 2007*, Lausanne, Switzerland, Nov. 2007.
[2] The Glomosim webpage, http://pcl.cs.ucla.edu/projects/glomosim/.
[3] S. Katti, H. Rahul, W. Hu, D. Katabi, M. Medard, J. Crowcroft, "XORs in The Air: Practical Network Coding," *in Proc. of ACM SIGCOMM*, 2006.
[4] H. Seferoglu, O. Gurbuz, O. Ercetin, Y. Altunbasak, "Video Streaming to Multiple Clients over Wireless Local Area Networks," *in Proc. of IEEE ICIP*, Atlanta, GA, Oct. 2006.

Progress Report on MIMO System Design With Receive Polarization Diversity: Fall 2007

Volkan Sevindik, Advisor: Ender Ayanoglu
Center for Pervasive Communications and Computing
Department of Electrical Engineering and Computer Science
The Henry Samueli School of Engineering
University of California, Irvine
Irvine, California 92697-2625
Email: vsevindi@uci.edu

I. Introduction

Diversity techniques are widely used to combat the effects of wireless fading channels. The replicas of the same information bits are received in the receiver. It is less likely that all replicas of the same information will be in deep fading simultaneously. The most commonly used diversity techniques [6] are *frequency diversity* where signals are transmitted on different frequencies, *time diversity* where signals are transmitted at different times, *space diversity* [1] where signals are transmitted and/or received by multiple antennas. *polarization diversity* [2] where signals are transmitted/received with different polarization directions of antennas, *angle diversity* where signals are received by directional antennas.

The most obvious approach to diversity is the use of spatially separated antennas (*space diversity*). *Space diversity (antenna diversity)* is one of the key techniques to reduce the effect of multipath fading in wireless systems [1] - [5]. One can use multiple antennas at the transmitter/receiver which is called *transmit diversity* and *receive diversity* respectively.

II. Problem Definition

In MIMO system, in order to fully exploit diversity, spacing between adjacent antenna elements at the transmitter and receiver sides should be at least 10 - 15 wavelengths and 3 - 5 wavelengths respectively. From implementation point of view, it is hard to have multiple antennas with enough spacings at wireless handheld devices which are getting smaller day by day.

Therefore, we focus on designing MIMO system that implements polarization diversity at only the receiver side. In other words, we use uni-polarized antennas at the transmitter side, but dual-polarized antennas at the receiver side because of the space limitations. The channel model is different when the system employs polarization diversity. In our work, we will use the channel model given in [2], which is

$$\mathbf{H} = \sqrt{\frac{K}{1+K}}\bar{\mathbf{H}} + \sqrt{\frac{1}{1+K}}\tilde{\mathbf{H}} \tag{1}$$

In the case of *polarization diversity*, the channel matrix $\mathbf{H}$ can be decomposed into fixed and variable component as it is seen from channel definition. In this definition, K specifies fading characteristic of the channel that takes value between 0 and 10. K=0 corresponds to the pure *Rayleigh* fading and K $\neq$ 0 corresponds to the *Ricean* Fading.

In [2], the performance of Alamouti scheme is analyzed under receive antenna and transmit antenna polarization diversity. The input-output relation is given as [2],

$$\widetilde{r}_i = \sqrt{E_s}||\mathbf{H}||_F^2 s_i + \widetilde{n}_i, \qquad i = 0,1 \tag{2}$$

where $\widetilde{r}_i$ is the scalar processed received signal corresponding to transmitted symbol s_i (i=0,1), and $\widetilde{n}_i$ is a scalar zero-mean complex gaussian noise with variance $\varepsilon\{|\widetilde{n}_i|^2\} = ||\mathbf{H}||_F^2\sigma_n^2$, and $||\mathbf{H}||_F^2$ is the squared Frobenius norm of the channel matrix [2].

We will first make MIMO system simulations that are defined in [2], in order to make fair comparisons with the simulation results of the new MIMO system. Our main purpose is to analyze the performance of MIMO system under only receive antenna polarization diversity by using different space-time coding techniques [5] - [7], and to use soft decoding receiver structure in order to exploit the information in correlated received symbols.

References

[1] Alamouti, S. M., "A Simple Trannsmit Diversity Technique for Wireless Communications", *IEEE J. Select. Areas Commun.*, Vol. 16, No. 8, pp. 1451-1458, October 1998.
[2] Nabar, R. U., H. Bölcskei, V. Erceg, D. Gesbert and A. J. Paulraj, "Performance of Multiantenna Signaling Techniques in the Presence of Polarization Diversity", *IEEE Trans. Signal Process.*, Vol. 50, No. 10, pp. 2553-2562, October 2002.
[3] Nabar, R. U., H. Bölcskei, V.Erceg, D. Gesbert and A. J. Paulraj, "Diversity and Outage Performance in Space-Time Block Coded Ricean MIMO Channels", *IEEE Trans. Wireless Commun.*, Vol. 4, No. 5, pp. 2519-2532, September 2005.
[4] Paulraj, A. J., D. A. Gore, R. Nabar and H. Bölcskei, "An Overwiev of MIMO Communications -A Key to Gigabit Wireless", *Proc. IEEE*, Vol. 92, No. 2, pp. 198-218, February 2004.
[5] Tarokh, V., N. Seshadri and A. R. Calderbank, "Space-time Codes for High Data Rate Wireless Communication:Performance Criterion and Code Construction", *IEEE Trans. Inform. Theory*, Vol. 17, No. 3, pp. 451-460, March 1999.
[6] Tarokh, V., H. Jafarkhani and A. R. Calderbank, "Space-time Block Coding for Wireless Communications:Performance Results", *IEEE J. Select. Areas Commun.*, Vol. 16, No. 8, pp. 1451-1458, October 1998.
[7] Uysal, M. and C. Georghiades, "On the error performance analysis of space-time trellis codes: an analytical framework", *Proc. IEEE WCNC*, pp. 99-104, July 2002.

Progress Report Fall 2007: Interference Alignment and Degrees of Freedom of Interference Channels under Channel Estimation Error

S. Surendran
Under the supervision of Prof. Syed A. Jafar
Center for Pervasive Communications and Computing
Department of Electrical Engineering and Computer Science
University of California, Irvine
Irvine, California, 92697, USA
Email: ssurendr@uci.edu

***Abstract*— Degrees of freedom, or multiplexing gain, is a fundamental measure of capacity characterization of a network. Capacity characterizations, and degrees of freedom, have been established for most centralized networks like the Multiple Access Channel (MAC) and Broadcast Channel (BC) with multiple antennas at both receivers and transmitters. However, most of the multiuser capacity results have been obtained assuming availability of perfect channel state information (CSI) at the transmitter and receiver. This may not be possible in practice, hence the issue of channel uncertainty assumes importance. In the case of Interference Channels (IC), an example of distributed networks, the situation is problematic. First, there are very few capacity characterization results even when perfect CSI is available. Interference alignment is a powerful technique to achieve significant degrees of freedom for the Interference Channel. However, perfect CSI is assumed. Our main objective is to characterize the effect of channel estimation error on interference alignment for Interference Channels. In particular, we wish to obtain scaling laws that govern the relationship between achievable degrees of freedom and channel estimation error.**

I. Problem Definition

Degrees of freedom, or spatial multiplexing gain, is a fundamental measure of capacity characterization of a network. Degrees of freedom is the slope of network capacity versus the logarithm of the Signal-to-Noise (SNR) ratio curve. Indeed, degrees of freedom, in most scenarios, is the number of non-interfering paths that can be obtained through coding/signal-processing at both the transmitters and receivers. Multiple antennas employed at both transmitters and receivers, leading to Multi-Input Multi-Output (MIMO) systems, provide spatial degrees of freedom. For instance, in a fundamental paper Foschini [1] has shown for a point-to-point MIMO channel, the capacity, in the high SNR-regime, capacity is given by:

$$C(SNR) = min(N_t, N_r)log(SNR) + O(1) \tag{1}$$

hence the degrees of freedom is given by minimum of N_t transmit antennas and N_r receive antennas.

Capacity characterizations, and degrees of freedom, have been obtained for most centralized networks like the MIMO Multiple Access Channel (MAC) and MIMO Broadcast Channel (BC) with multiple antennas. But the situation is different for finite decentralized networks like the Interference Channel (IC). In fact, capacity characterizations, similar to the ones obtained for MAC and BC, remain open problems. In the absence of precise results, researchers have focused on obtaining approximate results; an approximate characterization of the capacity region of the 2 user Interference Channel has been found [2]. While it is possible for a wireless network to have as many spatial dimensions as the number of transmitting and receiving antennas, distributed nature of the IC makes it difficult to resolve the spatial dimensions. Hence, obtaining the number of degrees of freedom for the IC is a non-trivial problem, leading to loose bounds on multiplexing gain [3] [4]. Note that all these results have been obtained under the assumption of perfect or accurate channel knowledge being available at both transmitter and receivers.

It has been established that dirty paper coding (DPC) achieves both the sum rate capacity and full capacity region for MIMO BC channels [5] [6]. Furthermore, sum rate capacity of MIMO BC achieves the same spatial multiplexing gain as a point-point MIMO systems, that is, when all the receivers are allowed to cooperate. However, in order to achieve these gains the transmitter in the MIMO BC has to have perfect or accurate channel state information (CSI). For instance, consider point-point MIMO channels: the quality of CSI available at the transmitter does not affect the slope of the capacity versus SNR curve, that is, the spatial multiplexing gain. On the other hand in the case of MIMO BC the level of CSI affects the multiplexing gain [5]. Indeed, consider the case of a MIMO BC using zero forcing transmission and each receiver having perfect channel information. The transmitter is provided with quantized channel information. A key finding in [7] is: To achieve full multiplexing gain the feedback rate per user must increase linearly with SNR. However, no explicit relationship between channel estimation error and multiplexing gain is provided in [7].

Effect of channel estimation error on capacity and power allocation of fading point-to-point MIMO channels has been investigated in [8]. Hassibi and his co-workers have looked into the effects of channel estimation error on the capacity of MIMO BC [9] [10] [11]. In [10] a Multi-Input Single-Output

(MISO) channel is considered. There are M transmit antennas and n single-antenna users. The key finding is sum capacity is of the order $M \log\log(n)$, when the estimation error is of fixed variance and n is large. While the multiplexing gain is preserved there is a penalty in sum capacity.

II. INTERFERENCE ALIGNMENT/CHANNEL ESTIMATION ERROR: FUTURE PLANS

Interference alignment is a simple yet effective technique whereby the signal vectors can be aligned in a prescribed manner such that they 'cancel' each other at receivers where they constitute interference yet are resolved at receivers where they are desired signals. Interference alignment has been used to demonstrate the achievability of all points within the degrees of freedom of the MIMO X channel [12]. Cadambe and Jafar's work [13] forms the basis of this research. They have shown, among other things, the following key results:

- *The number of degrees of freedom for the K user interference channel with single antennas at all nodes is* $K/2$*.*
- *For the 3 user MIMO Interference Channel,* $3M/2$ *degrees of freedom can be obtained with constant channel matrices with* $M > 1$ *antennas at each node.*

Interference alignment assumes that all channel coefficients are known *a priori* to all transmitters and receivers. We consider the following channel error model. Given channel matrices $H^{[ij]}$ from transmitter j to receiver i, entries of these matrices are independent, identically distributed (i.i.d) and zero-mean circularly symmetric complex Gaussian (ZMCSCG). We employ genie-based minimum mean square estimation (MMSE) of $H^{[ij]}$. The estimation error is $E^{[ij]} = H^{[ij]} - \hat{H}^{[ij]}$, where $\hat{H}^{[ij]}$ is an estimate of $H^{[ij]}$. $E^{[ij]}$ and $\hat{H}^{[ij]}$ are uncorrelated by virtue of MMSE estimation, and the entries of $E^{[ij]}$ are ZMCSCG with a variance $\sigma_{\mathbf{E}}^2$. Also the entries of $\hat{H}^{[ij]}$ are i.i.d ZMCSCG with a variance $1 - \sigma_{\mathbf{E}}^2$ [8].

The interference alignment procedure will be analyzed under aforementioned channel estimation error model, where $\sigma_{\mathbf{E}}^2$ characterizes the quality of channel estimation. We hope to answer the following questions:

- *How does interference alignment perform when there is less than perfect channel information? What is the effect on achievable degrees of freedom in the the case of both* K *User IC and MIMO IC?*
- *What is the precise scaling relationship between* $\sigma_{\mathbf{E}}^2$ *and degrees of freedom in both cases?*

REFERENCES

[1] G. J. Foschini, "Layered space-time architecture for wireless communication in a fading environment when using multi-element antennas," *Bell Labs Tech. J*, vol. 1, no. 2, pp. 41–59, 1996.

[2] R. Etkin, D. Tse, and H. Wang, "Gaussian Interference Channel Capacity to within one Bit," *submitted to IEEE Trans. Inform. Theory*, Feb. 2007.

[3] A. Host-Madsen and A. Nosratinia, "The multiplexing gain of wireless networks," *in Proc. of ISIT*, 2005.

[4] A. Host-Madsen, "Capacity Bounds for Cooperative Diversity," *IEEE Trans. Inform. Theory*, vol. 52, pp. 1522–1544, Apr. 2006.

[5] G. Caire and S. Shamai, "On the achievable throughput of a multiantenna gaussian broadcast channel," *IEEE Trans. Inform. Theory*, vol. 49, pp. 1691–1706, July 2003.

[6] H.Weingarten, Y. Steinberg, and S. Shamai, "The Capacity Region of the Gaussian Multi-Input Multi-Output Broadcast Channel," *IEEE Trans. Inform. Theory*, vol. 52, pp. 3936–3964, Sept. 2006.

[7] N. Jindal, "MIMO Broadcast Channels with Finite Rate Feedback," *IEEE Trans. Inform. Theory*, vol. 52, pp. 5045–5059, Nov. 2006.

[8] T. Yoo and A. Goldsmith, "Capacity and Power Allocation for Fading MIMO Channels with Channel Estimation Errror," *IEEE Trans. Inform. Theory*, vol. 52, pp. 2203–2213, May 2006.

[9] M. Sharif and B. Hassibi, "On the Capacity of MIMO Broadcast Channels with Partial Channel State Information," *IEEE Trans. Inform. Theory*, vol. 51, pp. 506–522, Feb. 2005.

[10] A. F. Dana, M. Sharif, and B. Hassibi, "On the Capacity Region of Multi-antenna Gaussian Broadcast Channels with Estimation Error," *IEEE Inter. Symp. Info. Theory*, 2006.

[11] A. Vakili, M. Sharif, and B. Hassibi, "The Effect of Channel Estimation Error on the Throughput of Broadcast Channels," *Proceedings of the 2006 IEEE International Conference on Acoustics, Speech and Signal Processing.*

[12] S. A. Jafar and S. Shamai, "Degrees of Freedom Region for the MIMO X channel," *IEEE Trans. Inform. Theory*, vol. 54, pp. 151–170, Jan. 2008.

[13] V. R. Cadambe and S. A. Jafar, "Interference Alignment and the Degrees of Freedom for the K User Interference Channel," *arXiv: 0707.0323, preprint*.